A spectroscopic hike in the U–O phase diagram

Damien Prieur, Marie-Margaux Desagulier, Daniel R Neuville, Christine Guéneau, Enrica Epifano, Kathy Dardenne, Joerg Rothe, Philippe Martin

Submission to Journal of Synchrotron Radiation

A spectroscopic hike in the U-O phase diagram

Damien Prieur[1,2], Marie-Margaux Desagulier[3], Daniel R. Neuville[4], Christine Guéneau[5], Enrica Epifano[6], Kathy Dardenne[7], Joerg Rothe[7], Philippe Martin[3]*

[1] Helmholtz Zentrum Dresden-Rossendorf (HZDR), Institute of Resource Ecology, PO Box 510119, 01314 Dresden, Germany.

[2] The Rossendorf Beamline at ESRF—The European Synchrotron, CS40220, 38043 Grenoble Cedex 9, France

[3] CEA, DES, ISEC, DMRC, University of Montpellier-, Marcoule, France

4 Université de Paris, Institut de physique du globe de Paris, CNRS, 75238 Paris cedex 05

[5] Université Paris-Saclay, CEA, Service de la Corrosion et du Comportement des Matériaux dans leur Environnement (SCCME), 91191, Gif-sur-Yvette, France

[6]

[7] Karlsruhe Institute of Technology (KIT), Institute for Nuclear Waste Disposal (INE), P.O. Box 3640, D-76021 Karlsruhe, Germany

KEYWORDS: UO_2, *in situ* XANES, Thermodynamical Calculation, CALPHAD method

ABSTRACT

The U-O phase diagram is of paramount interest for nuclear related applications and has therefore been extensively studied. Experimental data has been gathered to feed the thermodynamical calculations and achieve an optimization of the U-O system modelization. Although considered as well established, a critical assessment of this large body of experimental data is necessary, especially in light of the recent development of new techniques applicable to actinide materials. Here we show how *in situ* XANES is suitable and relevant for phase diagram determination. New experimental data points have been collected using this method and discuss in regard to the available data. Comparing our experimental data with thermodynamical calculations, we observe that the current version of the U-O phase diagram misses some experimental data in specific domains. This lack of experimental data generates inaccuracy in the model, which can be overcome using *in situ* XANES. Indeed, as shown in the paper, this method is suitable to collect experimental data in non-ambient conditions and for multiphasic system.

INTRODUCTION

As for any element of the periodical table, actinide oxides chemistry, physics, thermodynamics and material science depend on the oxidation states. In the actinide series, uranium is of foremost importance in regards to its technological significance in nuclear-related applications [1]. Among the variety of stoichiometric and non-stoichiometric U oxides, uranium exists in the +III, +IV, +V and +VI oxidation states [2]. One of the key scientific challenges is a precise determination of uranium valence state as it dictates the oxides behaviour: from their irradiation in nuclear reactor to their disposal in dedicated waste repositories (fuel thermo-physical properties, chemical reactivity in the environment, *etc*.). Thanks to its element-specificity and local bonding–sensitivity, X-ray

Absorption Near Edge Structure (XANES) is a well-recognized method to assess the valence of almost any elements [3–5]. Applying this synchrotron technique at room temperature has become quite standard for some of the actinides (Th, U and Pu) in several dedicated beamlines [2,5–8]. However, some of the afore-mentioned processes are occurring in chemical (pH, etc.) or thermodynamical (temperature, oxygen partial pressure, etc.) conditions which may vary from the ambient ones and would require then an *in situ* determination of the oxidation state. Unfortunately, such *in situ* studies remains very scarce in reason of the safety issues associated with the handling of radionuclides-bearing samples in non-ambient conditions. In this context, the first goal of this paper is to show both feasibility and suitability of *in situ* L_{III} XANES applied to uranium oxides.

As a representative and comprehensive example, this article will present our spectroscopic hike into the U-O phase diagram. This system has been extensively studied in the past decades and the current version of its phase diagram is provided in the Figure 1 [9]. The experimental data, on which are based the thermochemical modelling, are also given. As noted in the phase diagram, the stable oxide phases are $UO_{2\pm x}$, U_4O_9, U_3O_7, U_3O_8 and UO_3.

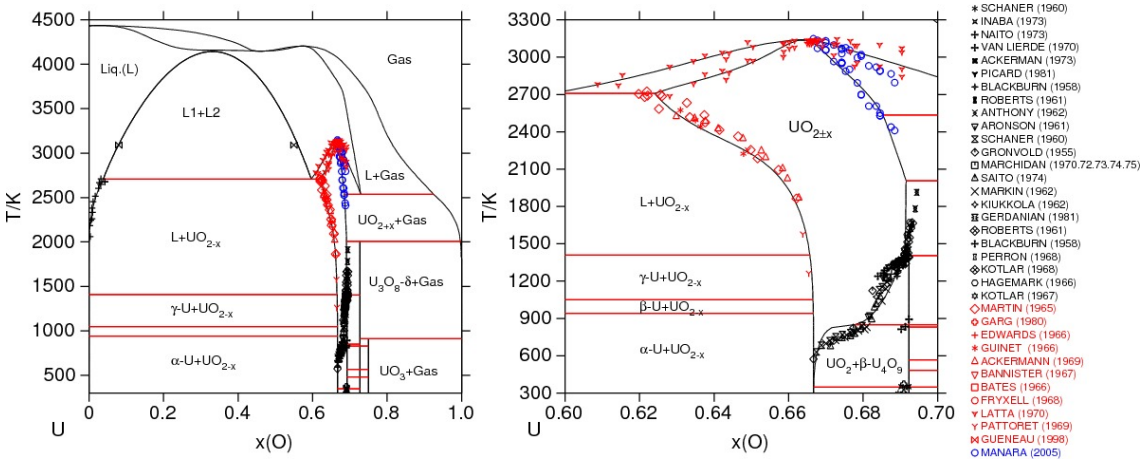

Figure 1: U-O Phase diagram calculated using the CALPHAD thermochemical modelling by Guéneau *et al.* [9] with the thermodynamic database TAF-ID in the whole O range (a) and restrained to 60 and 75 at.% O (b). Experimental data (red, black and blue points) and associated references are detailed in Baichi *et al.* [10], Labroche *et al.* [11] and Manara *et al.* [12] (Figure from Guéneau *et al.* [9])

Relatively to the UO_2 fuel, the most critical parameter to asses is the deviation from stoichiometry which is noted "x" and is specifically the gap from a O/U ratio equal to 2.00. In the U-O phase diagram, most of the O/U ratio have been derived from either X-ray diffraction (XRD) or thermogravimetric analysis (TGA). Contrary to XRD, TGA measures directly the oxygen content variation through the sample mass loss. However, accurate measurements require knowing either the initial or the final O/M of the studied compounds. In the case of XRD, the oxygen stoichiometry is indirectly derived from the lattice parameter using empirical relation [13]. This methodology is generally wrongly used in the UO_2 – U_4O_9 domain where two oxide phases may coexist[14]. Another drawback of XRD for this type of study lies in its limited resolution: the formation of higher U oxides is associated to a complex modification of the oxygen sub lattice, which cannot be properly discriminated. Additionally, one of the fundamental postulate, used for phase diagram assessment, is that U_4O_9, U_3O_7 and U_3O_8 are stoichiometric compounds while non-stoichiometry may exist in these oxide phases. On the other hand, XANES probes directly the valence state (unfilled *6d* and *5f* shells) of the cation through *2p-6d* transition ($L_{II,III}$ edge) and the associated oxygen stoichiometry is derived applying the electroneutrality rule. This technique appears then as a method of choice as illustrated by its application at room temperature for lanthanides- and actinides-doped UO_2 compounds [15–18]. Nevertheless, *in situ* XANES application to U oxides remains extremely rare and

has been limited to the UO_2-UO_{2+x} domain [19,20]. In this context, the second goal of this paper is to show the relevance of *in situ* XANES for such phase diagram determination. In this framework, new experimental data points have been collected using this method and discuss in regard to the available data. Furthermore, thermodynamic modelling have been performed using the CALPHAD (CALculation of PHAse Diagram) method permit to conclude about the relevance of those XANES-derived results.

EXPERIMENTAL METHODS

In situ X-ray Absorption Near Edge Structure

In situ XANES measurements were conducted on square (1.5x1.5 mm^2) samples extracted from a 0.5 mm thickness disk cut from a UO_2 dense pellet (98% of the theoretical density) sintered in Ar-4% H_2 at 2023 K during 4h. The surface exposed to the X-ray beam was polished up to a diamond finish and the samples were then annealed 4 h under a dry reducing atmosphere (Ar-5% H_2) atmosphere at 1673 K in order to remove damage induced by polishing and to guarantee an O/U ratio equal to 2.00.

Prior measurement, the sample is mounted on a 1 mm-diameter Pt/Ir (90/10) wire of the furnace and embedded in a Pt/Ir (90/10) foil with a 0.5 mm hole allowing the incoming X-Ray to hit the sample polished surface. Additional details on the sample positioning and a complete review of the heating wire can be found in Prieur *et al.* [19] and Neuville *et al.*[21], respectively. This heating element is then inserted into a dedicated furnace (Figure 2) which allows collecting *in situ* XAS data on radioactive samples in various atmospheres and up to 2000 K. The Pt/Ir wire temperature was calibrated before the measurement. This heating system has low thermal inertia and it is

possible to change the temperature from room temperature up to 2000K and the inverse as well in a few seconds.

During the measurements, a constant gas flow of 8 L/h was maintained using a Bronkhorst© numeric gas flow meter. The oxygen partial pressure in flowing gas was monitored by 1.2 bar mixing of Ar-4%H_2, Ar, Ar-100 ppm O_2 and 80%N_2-20%O_2 gas bottles. The oxygen partial pressure was continuously measured at the entrance of the furnace using a Jok'air device (SETNAG company). This equipment can measure $p(O_2)$ from 10^{-35} to 0.25 atm, and the provider indicates a relative uncertainty of 3% for this entire range; however, according to the repeatability of our experiences, higher uncertainties up to 20% should be considered for $p(O_2) < 10^{-6}$ atm.

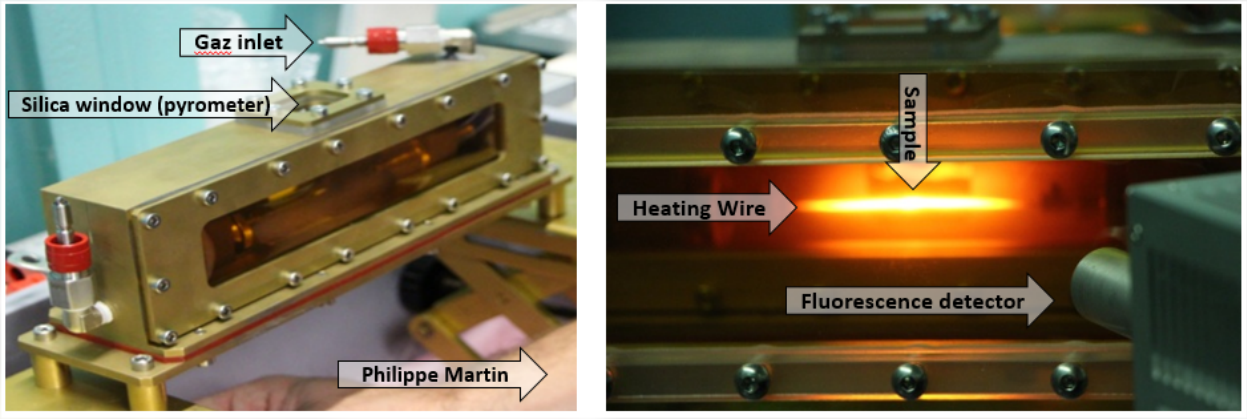

Figure 2: Pictures of the heating set up.

The *in situ* XANES measurements were conducted at the INE-Beamline of the KIT synchrotron light source (Karlsruhe Institute of Technology, Germany). The storage ring operating conditions were 2.5 GeV and 100-160mA. A Ge [422] double crystal monochromator coupled with collimating and focusing Rh-coated mirrors was used. XANES spectra were collected at in fluorescence mode at the U L_{III} edge (17166 eV) with a single element Si solid-state detector.

Energy calibration was achieved by measuring the K XANES spectrum of a Y reference foil (17038 eV) located between the second and third ionization chambers. The XANES spectra have been normalized using linear functions for pre- and post- edge modelling. The white-line maxima have been taken as the first zero-crossing of the first derivative. Pre-edge removal, normalization and self-absorption correction were performed using the ATHENA software [22]. The molar fractions of U^{IV}, U^{V} and U^{VI} were derived from the linear combination fitting (LCF) of stoichiometric $UO_{2.00}$, U_4O_9 and U_3O_8 references[15]. Note that this fitting procedure is not affected by the temperature. The XANES region is indeed quite insensitive to the thermal disorder, as it notably exhibit a high signal-to-noise ratio [19].

Thermodynamical modelling

The description of multicomponent systems is based on the assessments of simple subsystems using semi empirical models for the stable phase. These models permit to describe Gibbs energies as a function of temperature, composition and pressure in the CALPHAD approach [23,24]. In order to obtain the best fit with the available experimental data (crystallographic phases, oxygen potential, enthalpy, melting point, …), adjustable parameters are optimized. The thermodynamic modelling has been performed with the Thermo-Calc [24,25] software using for the calculation the TAF-ID database (Thermodynamic for Advanced Fuel – international data base release 11).

First, we calculated the binary phase diagram and the oxygen potential evolution in function of the O/U ratio for each test temperature using the thermodynamic assessment of Guéneau *et al.* [9].

Gibbs energy model

In the CALPHAD method, the thermodynamic equilibrium is calculated by minimizing the total Gibbs energy of the system, which is a linear combination of each Gibbs energy phase functions present in the system. These functions are described using the "sub-lattice model" proposed by Chevalier *et al.*[26,27] and Guéneau *et al.*[9] for the uranium-oxygen system. In this approach, the crystal structure of each phase known is decomposed in several sub-lattices and each one includes the different ionic species. Their relative different content is adjusted in order to respect the electrotroneutrality. The fluorite $UO_{2\pm x}$ structure can hence be described as follow:

$$(U^{3+},U^{4+},U^{6+})_1(O^{2-},Va)_2(O^{2-},Va)_1 \qquad (1)$$

where "Va" corresponds to the oxygen vacancies and the indexes 1 and 2 describe the stoichiometry of the compound.

As illustrated by the relation (1), the model is composed of one cationic sub-lattice and two anionic sub-lattices. One for the oxygen atoms on tetrahedral sites and the second one for oxygen atoms in the interstitial position. Thanks to the sub-lattice model, the compound Gibbs energy is determined for each phase. All the Gibbs energy functions refers to the Stable Element Reference (SER) corresponding to the standard state conditions (298.15K and 10^5 Pa) and they depend on the state variables such as temperature, composition and pressure leading to the general equation (2).

$$^{\circ}G_i^{\varphi}(T) - {}^{\circ}H_i^{SER}(298.15K) = a + bT + cTln(T) + \sum_n d_n T^n \qquad (2)$$

Furthermore, the Gibbs energy function is also written as the composition of different contributions, as followed:

$$G_m^{\varphi} - \sum_{i=A,B} x_i^{\varphi}\, {}^{\circ}H_i^{SER}(298.15K) = {}^{ref}G^{\phi} + {}^{id}G^{\phi} + {}^{ex}G^{\phi} \qquad (3)$$

In this function, ${}^{ref}G^{\phi}$ corresponds to the Gibbs energy of the reference state, ${}^{id}G^{\phi}$ to the ideal random mixing contribution and ${}^{ex}G^{\phi}$ to the excess of Gibbs energy. Concerning the ideal Gibbs energy, it depends on an interaction parameters between atoms A and B, noted $L_{A,B}^{\varphi}$. That parameters is

expressed with the Redlich-Krister polynome in order to describe more precisely all the experimental data [28]. All the Gibbs energy functions for each phases of the U-O system used in the TAF-ID are detailed in the assessment of Guéneau et al. [9].

Selection of oxygen potential data

The oxygen potential is the equilibrium between oxygen in the sample and oxygen in the gas phase and is defined as:

$$\mu(O_2) = RTln(pO_2/p^0) \quad (4)$$

with pO_2 the partial pressure of oxygen, p^0 the standard pressure, R the gas constant and T the temperature.

The different oxygen potential data sets critically selected by Labroche [11] and Baichi [10] and used in the assessment of Guéneau *et al.* [9] are summarized in **Erreur ! Source du renvoi introuvable.**. Those data correspond to partial pressure or oxygen potential for different temperatures, which stoichiometry have been derived from various characterization methods (*e.g.* XRD, TGA). As illustrated by the Figure 3 showing the comparison between experimental and calculated oxygen activities in $UO_{2\pm x}$ domain, the evolution of the oxygen potential considerably vary with the O/M ratio and temperature. Furthermore, this representation shows a lack of experimental data for specific domains, according to the O/M ratio and the temperature. Note that for temperatures lower than 800K, no data are available.

The experimental thermodynamic data sets available in the literature corresponding to conditions used for *in situ* XANES measurements: 298 (3), 448 (5), 773 (8), 1476 (15), 1483 (15), 1873 (19) and 1951 (20) K (a temperature range of ± 100K was considered) are summarized in the **Erreur ! Source du renvoi introuvable.**.

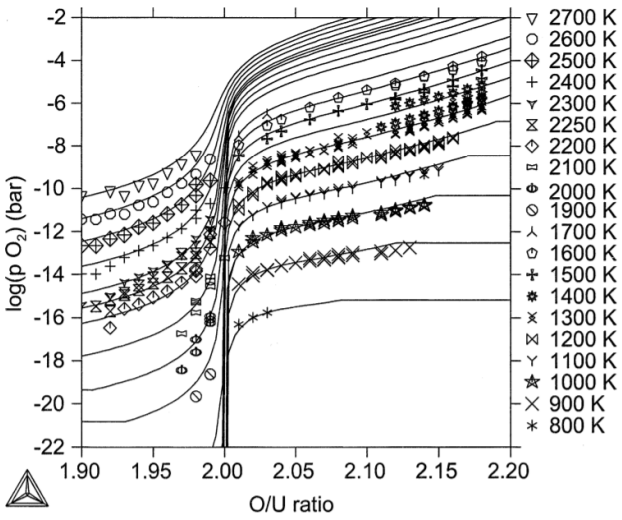

Figure 3: Oxygen activities in $UO_{2\pm x}$ calculated with selected experimental data from Guéneau *et al.* [9] (Figure from Guéneau *et al.* [9])

Table 1: Experimental U-O thermodynamic data selected by Guéneau et al. [9] for the assessment of the U-O system

Data	References
O chemical potential in UO_{2-x}	Tetenbaum *et al.* [29], Pattoret *et al.* [30], Javed *et al.*[31]
O chemical potential in UO_{2+x}	Gerdanian *et al.* [32], Kotlar *et al.* [33,34], Hagemark *et al.*[35], Roberts *et al.*[36], Blackburn *et al.*[37], Aronson *et al.*[38], Marchidan *et al.* [39], Markin *et al.* [40], Saito *et al.* [41], Kiukkola *et al.* [42], Nakamura *et al.* [43]
O chemical potential in UO_{2+x}/U_4O_9	Nakamura *et al.* [43], Kiukkola *et al.* [42], Markin *et al.* [40], Blackburn *et al.* [37](1958), Kotlar *et al.* [33,34]
O chemical potential in UO_{2-x}	Pattoret *et al.* [30], Baichi *et al.* [10]

Table 2: Experimental U-O thermodynamic data selected in this present work

Data	References	Temperature domain
O chemical potential in UO_{2+x}/U_4O_9	Hagemark *et al.* [35]	1500-1573K
	Roberts *et al.* [36]	1420-1500K
	Blackburn *et al.* [37]	1399-1500K
O chemical potential in UO_{2-x}	Javed *et al.* [31]	1900-2000K
	Pattoret *et al.* [30]	2000K
	Tetenbaum *et al.* [29]	2000K
O chemical potential in Liquid/UO_{2-x}	Pattoret *et al.* [30]	1950-2000K
	Baichi *et al.* [10]	1942-2000K

RESULTS AND DISCUSSION

Figure 4 presents the range of temperature and oxygen potential in which experimental data have already been collected. Comparing with our new experimental points, we observe that our study provides new experimental data and especially in condition domains which have not been studied before (temperature inferior to 800 K / oxygen potential of -100 $kJ.mol^{-1}$ and temperature superior to 1700 K).

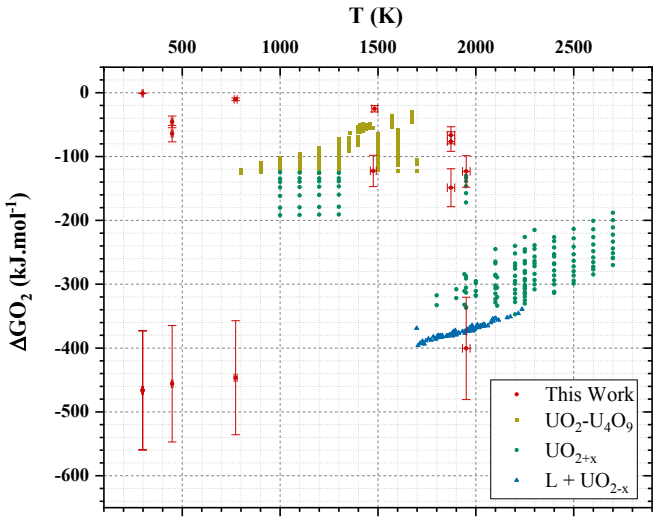

Figure 4: Oxygen potential (kJ.mol^{-1}) and temperature (K) of our experimental data and the experimental U-O thermodynamic data selected by Guéneau *et al.*[9]. Note that only bibliographic data corresponding to the range of our study has been plotted.

U L_{III} XANES spectra have been collected for each data points. Figure 5 (a) provides an example of XANES spectra recorded on a sample heated at 1873 (19) K in different atmospheres (*i.e.* -450 (90), -150 (30) and -50 (10) kJ.mol^{-1}). The sample heated in the most reducing conditions (dry Ar-H_2) is clearly stoichiometric because its white line is identical to the $UO_{2.00}$ reference. On the contrary, a shift toward higher energy, as well as a broadening, appears when heated in more oxidizing conditions (*i.e.* Ar and Air). These spectral changes indicate a modification of U oxidation state, and especially of oxidation in the present case. Note that the variation of intensity between the $UO_{2.00}$ reference and the experimental spectra is due to the increase of thermal vibrations.

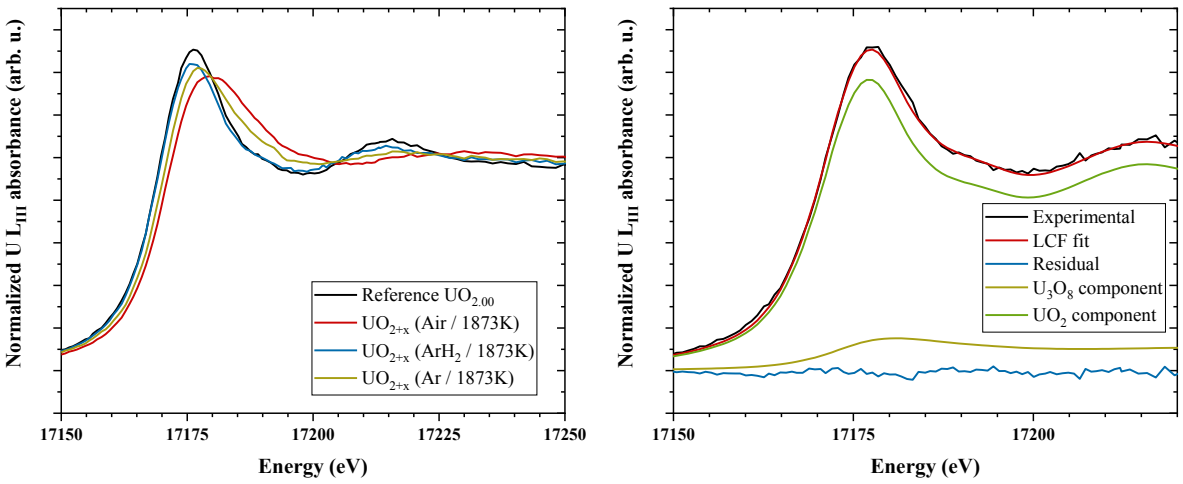

Figure 5: (a) UL_{III} XANES spectra of UO_{2+x} samples measured at 1873 (19) K in different oxygen potentials. (b) LCF of an UL_{III} XANES experimental spectrum fitted with UO_2 and U_3O_8 components.

The UL_{III} XANES spectra were fitted in order to determine the U valence and the corresponding molar fractions of each oxidation state. The basic principle of LCF is to fit the XANES experimental spectrum by combining XANES experimental spectra of reference materials. As an example, the Figure 5 (b) shows the fit of an experimental spectrum using two components: UO_2 and U_3O_8. The output of such procedure is the molar fractions of each component species, which allows deriving the molar fraction of U^{IV}, U^{V}, and U^{VI}, as well as the O/U ratio.

By plotting our O/U experimental values into the U-O phase diagram (Figure 6), we can observe that our data are scattered in different domains: UO_{2+x}, UO_2-U_4O_9 and UO_{2+x}-U_3O_8. It is remarkable to note that, for each collected experimental point, the best LCF results are systematically obtained using component species matching the end-members indicated in the phase diagram (*cf*. Table 1 of SI). For instance, the experimental spectrum of Figure 5 (b) has been fitted using UO_2 and U_3O_8;

and this experimental point is actually in the UO_{2+x} – U_3O_8 domain of the U-O phase diagram. This supports the validity of the LCF approach to determine the O/U value.

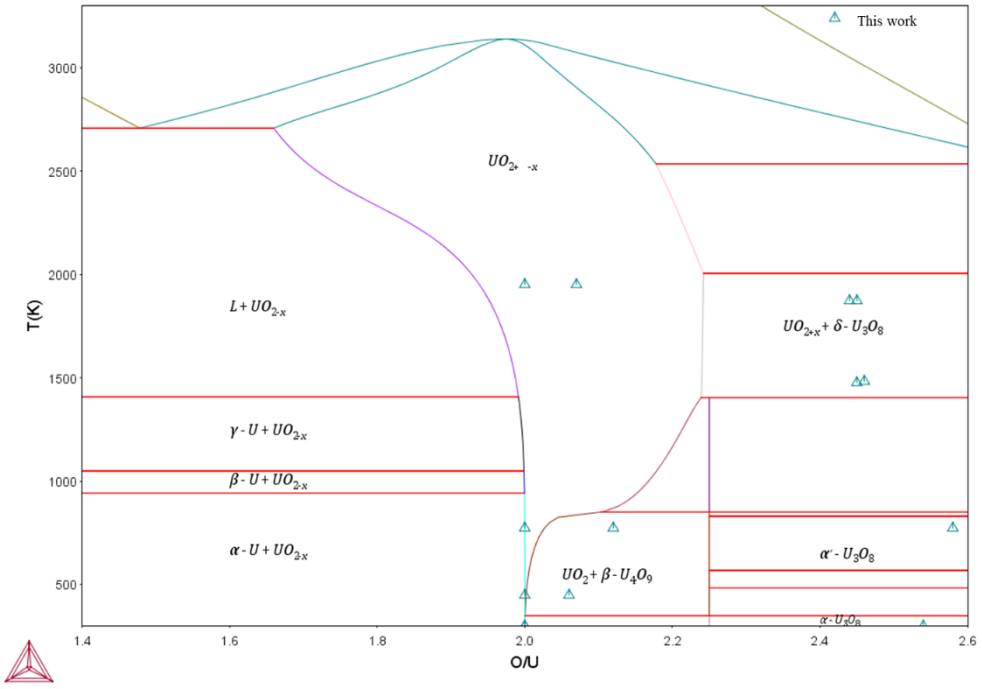

Figure 6: Our experimental point (blue triangle) in the calculated U-O phase diagram.

Figure 7 compare, for a given temperature, our experimental values (red circle) with the oxygen potential curve (black line) derived from the thermodynamical modelling. Note that the calculated data are extrapolated from the existing experimental data (green square) and the thermodynamic data of each U oxide end-members considered in CALPHAD model.

Overall, we observe two main tendencies: for T > 1400K, our data are in good agreement with the predicted values while a poor agreement is reached for T < 800K. This corresponds actually quite well with domains in temperature and oxygen potential with a lack of experimental data points. In detail, our 2 experimental points at 1951 (20) K are in a very good agreement with the model. This

can be understood from the fact that for this temperature the model is based on several experimental points ranging from O/U = 1.95 to O/M = 2.02 as illustrated by Table 2 and Figure 7, which allows a proper extrapolation for higher O/U values. At 1876 (19) K, our experimental data correspond to a domain of oxygen potential where no data has been reported in the literature. The tendency is respected but the O/U values predicted by the model are much lower than the experimental data. For both 1476 (15) and 1483 (15) K, both experimental and calculated values are consistent. At lower temperature, *i.e*. 448 (5) and 773 (8) K, there is a perfect agreement for the stoichiometric values while experimental and calculated data does not match for higher O/U values. In that case, the kinetic of the reaction might play a role in the final O/U value but, undoubtedly, the main problem comes from the absence of experimental data in this conditions domain.

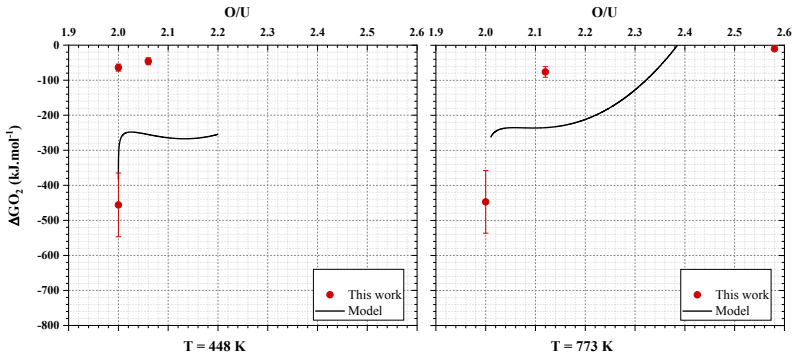

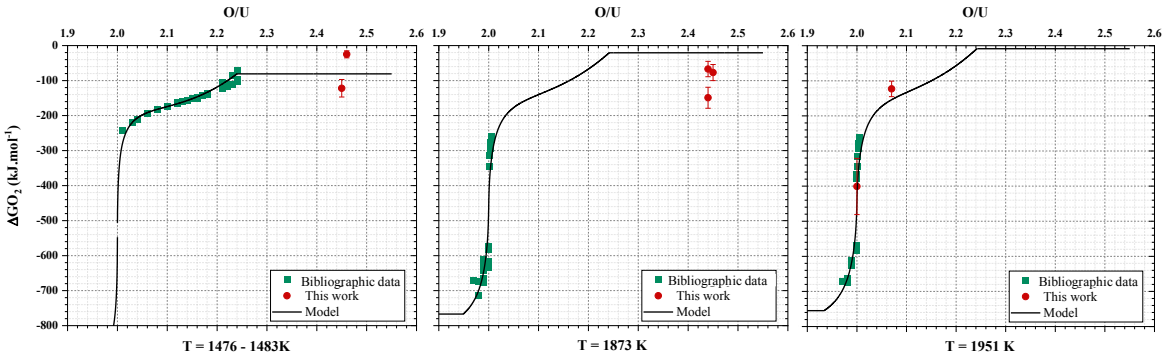

Figure 7: For T>1400K, comparison between the O/U calculated (black line) and our experimental data (yellow circle), and the selected experimental data (colored square) Note that the oxygen potential curves (black line) are solely based on the experimental data from literature (colored square).

CONCLUSION

In this study, *in situ* XANES has been used to explore the U-O phase diagram and to collect new experimental data in condition domains in which experimental data were missing. *In situ* XANES is particularly relevant for such purpose as, contrary to other methods, O/U can be determined independently of the crystallographic nature of the samples. Those new experimental results could be used to optimize the thermochemical model in the CALPHAD approach.

By itself, in situ method has already a huge interest for a wide range of applications in which the oxidation states drive the chemical processes. But here we also demonstrated that *in situ* XANES, coupled with thermodynamical calculation, is a proper combination to assess phase diagram. Indeed, *in situ* XANES allows collecting relevant data close to the real thermodynamic conditions encountered in the nuclear fuel cycle.

Combining it with x-ray diffraction for example would of course unravel even more fruitful informations, as one would be able to access both charge distribution and phase structure at the same time.

AUTHOR INFORMATION

Corresponding Authors

*E-mail: d.prieur@hzdr.de

Conflicts of interest

There are no conflicts to declare.

ACKNOWLEDGMENT

D. P. and P.M. acknowledge the KIT light source for provision of instruments at their beamlines and the Institute for Beam Physics and Technology (IBPT) for the operation of the storage ring, the Karlsruhe Research Accelerator (KARA).

REFERENCES

(1) Burns, P. C.; Ewing, R. C.; Navrotsky, A. Nuclear Fuel in a Reactor Accident. *Science* **2012**, *335* (6073), 1184–1188. https://doi.org/10.1126/science.1211285.

(2) Kvashnina, K. O.; Butorin, S. M.; Martin, P.; Glatzel, P. Chemical State of Complex Uranium Oxides. *Phys. Rev. Lett.* **2013**, *111* (25), 253002. https://doi.org/10.1103/PhysRevLett.111.253002.

(3) Denecke, M. A. Actinide Speciation Using Synchrotron-Based Methods. *J Radioanal Nucl Chem* **2015**, *303* (2), 1339–1343. https://doi.org/10.1007/s10967-014-3493-3.

(4) Shi, W.-Q.; Yuan, L.-Y.; Wang, C.-Z.; Wang, L.; Mei, L.; Xiao, C.-L.; Zhang, L.; Li, Z.-J.; Zhao, Y.-L.; Chai, Z.-F. Exploring Actinide Materials Through Synchrotron Radiation Techniques. *Advanced Materials* **2014**, *26* (46), 7807–7848. https://doi.org/10.1002/adma.201304323.

(5) Rothe, J.; Butorin, S.; Dardenne, K.; Denecke, M. A.; Kienzler, B.; Löble, M.; Metz, V.; Seibert, A.; Steppert, M.; Vitova, T.; Walther, C.; Geckeis, H. The INE-Beamline for Actinide Science at ANKA. *Review of Scientific Instruments* **2012**, *83* (4), 043105. https://doi.org/10.1063/1.3700813.

(6) Fortner, F. A.; Kropf, A. J.; Cunnane, J. C. *The Chemistry Os Spent Nuclear Fuel From X-Ray Absorption Spectroscopy*; NA; Yucca Mountain Project, Las Vegas, NV (United States), 2006. https://doi.org/10.2172/899267.

(7) Denecke, M. A. X-Ray Spectroscopy in Studies of the Nuclear Fuel Cycle. In *X-Ray Absorption and X-Ray Emission Spectroscopy*; John Wiley & Sons, Ltd, 2016; pp 523–559. https://doi.org/10.1002/9781118844243.ch19.

(8) Scheinost, A. C.; Claussner, J.; Exner, J.; Feig, M.; Findeisen, S.; Hennig, C.; Kvashnina, K. O.; Naudet, D.; Prieur, D.; Rossberg, A.; Schmidt, M.; Qiu, C.; Colomp, P.; Cohen, C.; Dettona, E.; Dyadkin, V.; Stumpf, T. ROBL-II at ESRF: A Synchrotron Toolbox for Actinide Research. *JOURNAL OF SYNCHROTRON RADIATION*, 2021, *28*, 333–349. https://doi.org/10.1107/S1600577520014265.

(9) Guéneau, C.; Baichi, M.; Labroche, D.; Chatillon, C.; Sundman, B. Thermodynamic Assessment of the Uranium–Oxygen System. *Journal of Nuclear Materials* **2002**, *304* (2–3), 161–175. https://doi.org/10.1016/S0022-3115(02)00878-4.

(10) Baichi, M.; Chatillon, C.; Ducros, G.; Froment, K. Thermodynamics of the O–U System: III – Critical Assessment of Phase Diagram Data in the U–UO2+x Composition Range. *Journal of Nuclear Materials* **2006**, *349* (1), 57–82. https://doi.org/10.1016/j.jnucmat.2005.10.001.

(11) Labroche, D.; Dugne, O.; Chatillon, C. Thermodynamic Properties of the O–U System. II – Critical Assessment of the Stability and Composition Range of the Oxides UO2+x, U4O9–y and U3O8–z. *Journal of Nuclear Materials* **2003**, *312* (1), 50–66. https://doi.org/10.1016/S0022-3115(02)01323-5.

(12) Manara, D.; Ronchi, C.; Sheindlin, M.; Lewis, M.; Brykin, M. Melting of Stoichiometric and Hyperstoichiometric Uranium Dioxide. **2005**.

(13) Ohmichi, T.; Fukushima, S.; Maeda, A.; Watanabe, H. On the Relation between Lattice Parameter and O/M Ratio for Uranium Dioxide-Trivalent Rare Earth Oxide Solid Solution. *Journal of Nuclear Materials* **1981**, *102*, 40–46. https://doi.org/10.1016/0022-3115(81)90544-4.

(14) Elorrieta, J. M.; Bonales, L. J.; Rodríguez-Villagra, N.; Baonza, V. G.; Cobos, J. A Detailed Raman and X-Ray Study of UO2+x Oxides and Related Structure Transitions. *Phys. Chem. Chem. Phys.* **2016**, *18* (40), 28209–28216. https://doi.org/10.1039/C6CP03800J.

(15) Prieur, D.; Martin, P. M.; Jankowiak, A.; Gavilan, E.; Scheinost, A. C.; Herlet, N.; Dehaudt, P.; Blanchart, P. Local Structure and Charge Distribution in Mixed Uranium-Americium Oxides: Effects of Oxygen Potential and Am Content. *Inorg. Chem.* **2011**, *50* (24), 12437–12445. https://doi.org/10.1021/ic200910f.

(16) Prieur, D.; Martin, P.; Lebreton, F.; Delahaye, T.; Banerjee, D.; Scheinost, A. C.; Jankowiak, A. Accommodation of Multivalent Cations in Fluorite-Type Solid Solutions: Case of Am-Bearing UO2. *J. Nucl. Mater.* **2013**, *434* (1–3), 7–16. https://doi.org/10.1016/j.jnucmat.2012.11.037.

(17) Martin, P.; Ripert, M.; Petit, T.; Reich, T.; Hennig, C.; D'Acapito, F.; Hazemann, J. L.; Proux, O. A XAS Study of the Local Environments of Cations in (U, Ce)O2. *Journal of Nuclear Materials* **2003**, *312* (1), 103–110. https://doi.org/10.1016/S0022-3115(02)01590-8.

(18) Prieur, D.; Martel, L.; Vigier, J.-F.; Scheinost, A. C.; Kvashnina, K. O.; Somers, J.; Martin, P. M. Aliovalent Cation Substitution in UO2: Electronic and Local Structures of U1–YLayO2±x Solid Solutions. *Inorg. Chem.* **2018**. https://doi.org/10.1021/acs.inorgchem.7b02839.

(19) Prieur, D.; Epifano, E.; Dardenne, K.; Rothe, J.; Hennig, C.; Scheinost, A. C.; Neuville, D. R.; Martin, P. M. Peculiar Thermal Behavior of UO2 Local Stucture. *Inorg. Chem.* **2018**, *57* (23), 14890–14894. https://doi.org/10.1021/acs.inorgchem.8b02657.

(20) Caisso, M.; Picart, S.; Belin, R. C.; Lebreton, F.; Martin, P. M.; Dardenne, K.; Rothe, J.; Neuville, D. R.; Delahaye, T.; Ayral, A. In Situ Characterization of Uranium and Americium Oxide Solid Solution Formation for CRMP Process: First Combination of in Situ XRD and XANES Measurements. *Dalton Trans.* **2015**, *44* (14), 6391–6399. https://doi.org/10.1039/C4DT03515A.

(21) Neuville, D. R.; Hennet, L.; Florian, P.; Ligny, D. de. In Situ High-Temperature Experiments. *Reviews in Mineralogy and Geochemistry* **2014**, *78* (1), 779–800. https://doi.org/10.2138/rmg.2013.78.19.

(22) Ravel, B.; Newville, M. ATHENA, ARTEMIS, HEPHAESTUS: Data Analysis for X-Ray Absorption Spectroscopy Using IFEFFIT. *J Synchrotron Rad, J Synchrotron Radiat* **2005**, *12* (4), 537–541. https://doi.org/10.1107/S0909049505012719.

(23) Cacciamani, G. An Introduction to the Calphad Method and the Compound Energy Formalism (CEF). *Tecnologia em Metalurgia, Materiais e Mineração* **2016**, *13* (1), 16–24.

(24) Kattner, U. R. The CALPHAD Method and Its Role in Material and Process Development. **2016**, *13* (1), 3–15.

(25) Sundman, B.; Jansson, B.; Andersson, J.-O. The Thermo-Calc Databank System. *Calphad* **1985**, *9* (2), 153–190. https://doi.org/10.1016/0364-5916(85)90021-5.

(26) Chevalier, P. Y.; Fischer, E. Thermodynamic Modelling of the O–U–Zr System. *Journal of Nuclear Materials* **1998**, *257* (3), 213–255. https://doi.org/10.1016/S0022-3115(98)00450-4.

(27) Chevalier, P.-Y.; Fischer, E.; Cheynet, B. Progress in the Thermodynamic Modelling of the O–U Binary System. *Journal of Nuclear Materials* **2002**, *303* (1), 1–28. https://doi.org/10.1016/S0022-3115(02)00813-9.

(28) Redlich, O.; Kister, A. T. Algebraic Representation of Thermodynamic Properties and the Classification of Solutions. *Ind. Eng. Chem.* **1948**, *40* (2), 345–348. https://doi.org/10.1021/ie50458a036.

(29) Tetenbaum, M.; Hunt, P. D. Total Pressure of Uranium-Bearing Species over Oxygen-Deficient Urania. *Journal of Nuclear Materials* **1970**, *34* (1), 86–91. https://doi.org/10.1016/0022-3115(70)90010-3.

(30) Pattoret, A.; Drowart, J.; Smoes, S. Mass Spectrometric Determination of Heat of Sublimation of Uranium. *Trans. Faraday Soc.* **1969**, *65* (0), 98–112. https://doi.org/10.1039/TF9696500098.

(31) Javed, N. A. Thermodynamic Study of Hypostoichiometric Urania. *Journal of Nuclear Materials* **1972**, *43* (3), 219–224. https://doi.org/10.1016/0022-3115(72)90053-0.

(32) Gerdanian, P.; Dodé, M. Étude thermodynamique des oxydes UO2+x. *J. Chim. Phys.* **1965**, *62*, 171–184. https://doi.org/10.1051/jcp/1965620171.

(33) Kotlar, A.; Gerdanian, P.; Dodé, M. Détermination des pressions partielles d'oxygène en équilibre avec les oxydes non-stœchiométriques du système U — O pour 1 050 °C < θ < 1 150 °C et 2,19 < O/U < 2,63 - II. — Tracé des isothermes Po2 (O/U) pour 1 082 °C — 1 098 °C — 1 123° C — 1137 °C et 1 150 °C. Diagramme des phases. *J. Chim. Phys.* **1967**, *64*, 1135–1144. https://doi.org/10.1051/jcp/1967641135.

(34) Kotlar, A.; Gerdanian, P.; Dodé, M. Détermination des pressions partielles d'oxygène en équilibre avec les oxydes non-stœchiométriques du système U — O pour 1 080 < θ °C < 1 150 et 2,19 < O/U < 2,63 - I. —Tracé de l'isotherme PO2(O/U) à 1 098 °C. Essai d'interprétation de la complexité des phénomènes observés par analogie avec la théorie des

« petits systèmes » de Terrell L. HILL. *J. Chim. Phys.* **1967**, *64*, 862–868. https://doi.org/10.1051/jcp/1967640862.

(35) Hagemark, K.; Broli, M. Equilibrium Oxygen Pressures over the Nonstoicheiometric Uranium Oxides UO2+x and U3O8−z at Higher Temperatures. *Journal of Inorganic and Nuclear Chemistry* **1966**, *28* (12), 2837–2850. https://doi.org/10.1016/0022-1902(66)80010-6.

(36) Roberts, L. E. J.; Walter, A. J. Equilibrium Pressures and Phase Relations in the Uranium Oxide System. *Journal of Inorganic and Nuclear Chemistry* **1961**, *22* (3), 213–229. https://doi.org/10.1016/0022-1902(61)80437-5.

(37) Blackburn, P. E. Oxygen Dissociation Pressures over Uranium Oxides. *J. Phys. Chem.* **1958**, *62* (8), 897–902. https://doi.org/10.1021/j150566a001.

(38) Aronson, S.; Rulli, J. E.; Schaner, B. E. Electrical Properties of Nonstoichiometric Uranium Dioxide. *J. Chem. Phys.* **1961**, *35* (4), 1382–1388. https://doi.org/10.1063/1.1732057.

(39) Marchidan, D. I. *Study of the Thermal and Thermodynamic Properties of Uranium Compounds*; IAEA-R--695-F; International Atomic Energy Agency, 1972.

(40) Markin, T. L.; Bones, R. J. *The Determination of Some Thermodynamic Properties of Uranium Oxides with O/U Ratios Between 2.00 and 2.03 Using a High Temperature Galvinic Cell*; UK Atomic Energy Authority Research Group, 1962.

(41) Yasutoshi, S. Nonstoichiometry in Uranium Dioxide. *Journal of Nuclear Materials* **1974**, *51* (1), 112–125. https://doi.org/10.1016/0022-3115(74)90121-4.

(42) Kiukkola, K.; Yhland, M.; Krohn, C.; Motzfeldt, K.; Theander, O.; Flood, H. High-Temperature Electrochemical Study of Uranium Oxides in the UO2-U3O8 Region. *Acta Chemica Scandinavica (1989)* **1962**, *16*. https://doi.org/10.3891/acta.chem.scand.16-0327.

(43) Nakamura, A.; Fujino, T. Thermodynamic Study of UO2 +x by Solid State Emf Technique. *Journal of Nuclear Materials* **1987**, *149* (1), 80–100. https://doi.org/10.1016/0022-3115(87)90501-0.